RSC Advances

PAPER

View Article Online
View Journal | View Issue

Cite this: *RSC Adv.*, 2018, **8**, 655

Effect of C_{60} on the phase transition behavior of a lipid bilayer under high pressure

Haiyang Yang,[a] Zhiheng Huang[a] and Yong Zhang*[b]

Received 28th August 2017
Accepted 6th December 2017

DOI: 10.1039/c7ra09514g

rsc.li/rsc-advances

Interactions between fullerenes and cells and effects on the main transition of lipid bilayers have attracted much attention in biophysics in recent years. By employing coarse-grained molecular dynamics simulations, we obtained the temperature–pressure phase diagrams of a dipalmitoylphosphatidylcholine bilayer, which exhibits a gel phase and a fluid phase, with variation of the C_{60} *versus* lipid ratios. The simulation results show that the critical area per lipid at the fluid–gel main phase transition boundary increases with the increasing ratios of C_{60}. A critical area per lipid of 0.594 ± 0.002 nm^2 is obtained when the ratio of C_{60} reaches 6.4% while that of the pure bilayer case is 0.572 ± 0.002 nm^2. The main transition temperature, T_m, remains almost unchanged with the addition of C_{60} below a ratio of 4.7%, while a 2 K decrease of T_m is observed at a ratio of 6.4% under various pressures. Consequently, the presence of C_{60} in the bilayer, with the ratio of C_{60} less than 4.7%, will not influence the main transition behavior of the bilayer even under pressure as high as 1500 bar. The radial distribution function analyses suggest that the presence of C_{60} produces no impact on the radial distribution of the lipids in the bilayers. The lateral density profiles show that the incorporation of C_{60} with relatively high ratios stabilizes the thickness of the bilayer.

1 Introduction

Fullerenes have attracted attention extensively since C_{60} was first discovered in 1985.[1] They have various applications in diverse fields, *e.g.*, energy application,[2] cosmetic products,[3] medical application[4] and polymer modifications[5] due to their unique physicochemical properties.[6] In particular, tremendous efforts have been focused on the applications of fullerenes in biomedicine since the landmark work by Friedman and co-workers in 1993.[7] For example, fullerenes have been used as HIV inhibitors[8–10] and radical scavengers[11–13] in therapeutics and fullerene–biomolecule conjugates have been designed as drug-delivery systems.[14–16] In addition, C_{60} fullerene and its derivatives are remarkable triplet sensitizers, which can be used to produce highly reactive oxygen species for photodynamic therapy.[17,18] On the basis of the appealing characteristics and application prospects of fullerenes, there has been growing interest in the study of fullerenes and their interactions with biological systems, in particular with lipid bilayers.[19–25]

In a biological system, a biomembrane is one of the most fundamental structural elements, which acts as a highly selective barrier for the exchange of various molecules between different spatial regions and compartments. A lipid bilayer is usually employed as a simplified model of a biomembrane in the relevant studies. It is well known that the lipid bilayer exists in various phase states, depending on pressure, temperature, the lipid components and the ionic composition of the aqueous environment, *etc.* At high temperatures, the lipid molecules pack in a disordered state and form a flat fluid membrane called a fluid phase or a liquid-crystalline phase, which is mainly physiologically relevant. At low temperatures, on the contrary, the lipid molecules are densely compacted, forming a gel phase, which is characterized by ordered chains, a lower area per lipid (APL) and lower lipid lateral mobility compared to the fluid phase. The transition from the fluid phase to the gel phase with a temperature decrease is defined as the main transition, and the critical temperature of the main transition is called the main transition temperature (T_m). The main transition plays a vital role in biophysics for the reason that the shift of the T_m may exert remarkable influences on the biological activity of cell membranes and thus on interrupting the cell functions. For example, it has been reported that the physical state of lipid acyl chains produces a striking impact on the activity of membrane enzymes and the membrane transport processes.[26]

Experimental and simulation studies have confirmed that C_{60} can enter into lipid bilayers.[27–29] The effects of C_{60} on the physico-structural properties of lipid membranes have been investigated by Wong-Ekkabut and co-workers using computer simulations.[20] They reported an increase of bilayer viscosity and a 40% decrease of the lateral diffusion coefficient of the lipids. Meanwhile, the authors concluded that the addition of C_{60} has no obvious

[a]*School of Materials Science and Engineering, Sun Yat-Sen University, 135 West Xingang Road, Guangzhou 510275, China*
[b]*School of Physics, Sun Yat-Sen University, 135 West Xingang Road, Guangzhou 510275, China. E-mail: zhyong9@mail.sysu.edu.cn*

structural damage to the membrane since the phenomena of pore formation, micellization and bilayer rupture were not observed. Zhou *et al.* studied the effects of C_{60} on the mechanical resistance and elastic modulus of lipid bilayers using a combination of atomic force microscopy, laser scattering and infrared spectroscopy.[24] The results suggested that the incorporation of C_{60} weakens the lipid mobility in the gel phase and increases the membrane viscosity. Nevertheless, most of such studies focused on the effect of C_{60} on the mechanical and structural properties of the lipid membrane. Few studies have elucidated the effects of C_{60} on the main transition of the lipid membrane, in particular under high pressure.

Molecular dynamics (MD) simulations provide molecular-level insights into the mechanisms of various biological processes.[30] Many investigations on the main transition behavior of the lipid membrane using the MD simulation approach are successful.[31–34] In this study, we aim to explore the effects of C_{60} on the main transition behavior of the lipid bilayer and the distribution properties under high pressure. Using systematic coarse-grained (CG) MD simulations of fluid dipalmitoylphosphatidylcholine (DPPC) bilayers with various addition ratios of C_{60}, we obtain the relationship between T_m of the DPPC bilayer and the amount of C_{60} under different pressures and the T–p phase diagrams of the DPPC bilayer. Our results suggest that the presence of C_{60}, below a ratio of 4.7%, does not significantly influence the main transition behavior of the DPPC bilayer. However, the T_m of the DPPC bilayer decreases by about 2 K in the presence of 6.4% C_{60} under various pressures. In addition, the distribution properties of the DPPC molecules in the bilayer are discussed based on the radial distribution analyses and lateral density profiles to obtain further information of the effects of C_{60} on the DPPC bilayer.

2 Materials and methods

The Martini CG force field was employed in our dynamic simulations to study the effect of C_{60} on the main transition behavior and the relative distribution properties of the lipid bilayer under high pressure.[35,36] The initial DPPC bilayer coordinate file was obtained using the bilayer formation program insane.py provided by Wassenaar's group,[37] and the C_{60} particle coordinate file was from a previous model.[20] A particle free DPPC bilayer containing 264 lipids (132 lipids for each leaflet) and fully hydrated with 4130 CG water beads was placed in the simulation box with a dimension of $10 \times 9 \times 10$ nm^3. The C_{60}–bilayer systems were generated by mixing the C_{60} in a fully hydrated DPPC bilayer simulation box. One, four, eight, twelve and sixteen C_{60} particle(s) were added to the bilayer, corresponding to the C_{60}–DPPC ratios of 0.4%, 1.5%, 3.0%, 4.7% and 6.4%, respectively. The C_{60} particles were initially placed in the lipid tail regions to achieve an equilibrium state of the system as soon as possible. The CG models of a DPPC molecule, C_{60} particle and a snapshot of a DPPC bilayer with a number of C_{60} particles in an equilibrium state are shown in Fig. 1. All of the molecules in our CG-MD simulations were built up by various kinds of CG bead.

All MD simulations started from the fluid phase state and the C_{60}–DPPC bilayer systems were equilibrated at 325 K under ambient pressure for 3 μs. Then, the equilibrated patches under ambient pressure were coupled to higher pressures of 1, 300, 600, 1000 and 1500 bar, respectively, and equilibrated again for another 3 μs. The temperatures of the simulated equilibration at pressures lower than 300 bar were coupled to 325 K while the others were coupled to 370 K with an aim to obtain the fluid phase. The final equilibrated configurations corresponding to various higher pressures have been achieved for further simulations. All MD simulations were performed within the Gromacs 5.1.1 environment.[38,39] Periodic boundary conditions were applied, and the constant temperature and pressure conditions were achieved using the Berendsen algorithm.[40] The coupling constant of the temperature was 0.1 ps, while that of the pressure was 0.2 ps. We chose a semi-isotropic way for the pressure coupling to maintain a zero surface tension. Lennard-Jones (LJ) and electrostatic potentials were cut off at 1.1 nm. The time step

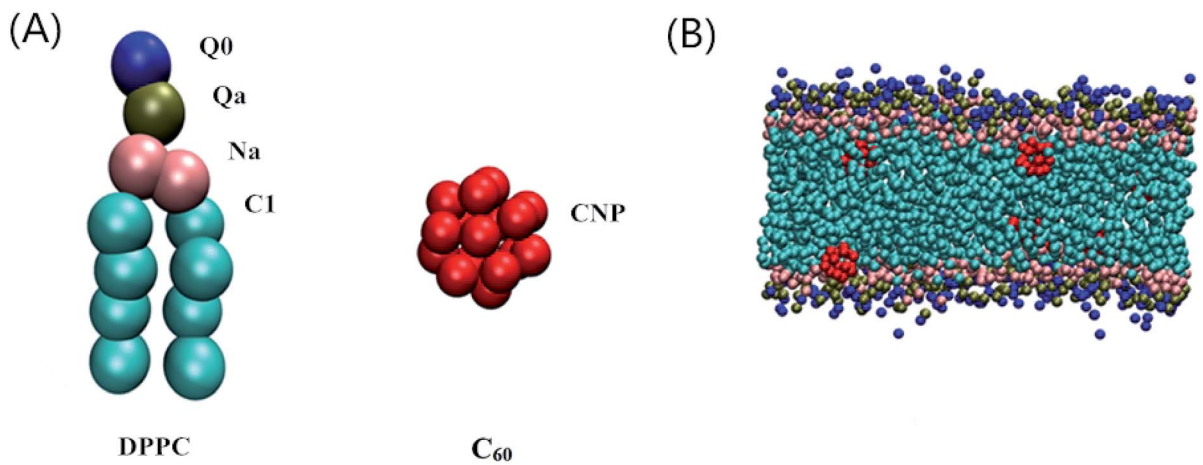

Fig. 1 (A) The CG models of DPPC and C_{60}. A DPPC molecule consists of 12 CG beads. The blue, green, pink and cyan beads represent the CG beads of the Q0, Qa, Na and C1 type, respectively. One C_{60} molecule consists of 16 CNP CG beads. (B) A snapshot of a DPPC bilayer with a number of C_{60} particles in an equilibrium state. For clarity, the CG water molecules are not shown.

of the simulations was fixed at 20 fs. Visual molecular dynamics (VMD) software,[41] version 1.9.2, was employed for the final visualization of the simulation results.

3 Results and discussion

3.1 APL

The APL is related to the tilt angle of the lipid tail and thus indicates the order of the acyl chain. The APL was calculated to investigate the progress of the main transition, as shown in Fig. 2. For the pure DPPC bilayer, a critical APL of 0.572 ± 0.002 nm^2 is found at the liquid–gel phase transition boundary, for which a value of 0.57 nm^2 has also been reported by Lai *et al.* through computer simulations for a pure DPPC membrane case.[31] The critical APL increases with the increasing ratio of C_{60} and it reaches 0.594 ± 0.002 nm^2 when the ratio of C_{60} increases to 6.4%. The results show that the incorporation of C_{60} in the DPPC bilayer increases the critical APL and an increment of 0.022 nm^2 is observed at a ratio of 6.4%. This suggests that the transition from the fluid phase to the gel phase becomes more difficult to take place. The value of 0.58 nm^2 was therefore used to determine whether the main transition has occurred or not in the following simulations, such that the T_ms corresponding to various pressures can be obtained.

3.2 Phase transition temperature

The T_ms of the pure DPPC bilayer under various external pressures are shown in Fig. 3. One can observe that the T_m increases when the pure DPPC bilayer is coupled to higher external pressures. The maximum difference in T_m between this work and the reported data is within 1 K, indicating a good agreement with the previous work.[31]

The main transition of the lipid bilayer at ambient pressure has been well studied by Marrink *et al.*[43] The calculated phase diagram of the DPPC bilayer is shown in Fig. 4. The same T_m of 289 K was found for the DPPC bilayers when the ratios of C_{60} are below 4.7% at ambient pressure. A corresponding value of 288 K has been reported by Lai *et al.*[31] and Ramalho *et al.*[33] in a pure DPPC bilayer case. The 1 K shift of the T_m is probably caused by thermal fluctuations and the differences in the system size and simulation time. At a ratio of 6.4%, the T_m decreases by about 2 K. In all of the simulations, the T_m increases with an increase in the external pressure, exhibiting a nonlinear relationship between the temperature T and the pressure p, which qualitatively agrees with the experimental data.[42] Our simulations show that the T_m of the DPPC bilayer will not be affected and the T–p phase diagram stays almost unchanged until the ratio of C_{60}

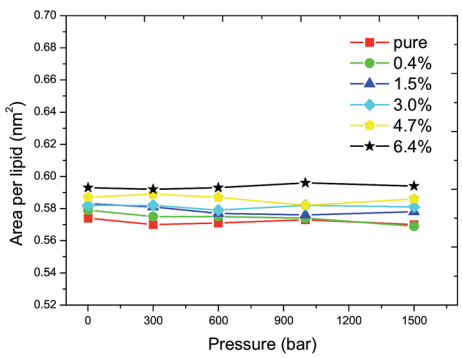

Fig. 2 The APL as a function of pressure at the main transition point. The red filled squares, green filled circles, blue filled triangles, cyan filled rhombuses, yellow regular pentagons and black pentagrams correspond to the ratios of C_{60} of 0%, 0.4%, 1.5%, 3.0%, 4.7% and 6.4%, respectively. A critical APL of 0.572 ± 0.002 nm^2 can be obtained for the pure DPPC bilayer. It increases to 0.594 ± 0.002 nm^2 when the ratio of C_{60} increases to 6.4%. This suggests that the main transition becomes more difficult to take place.

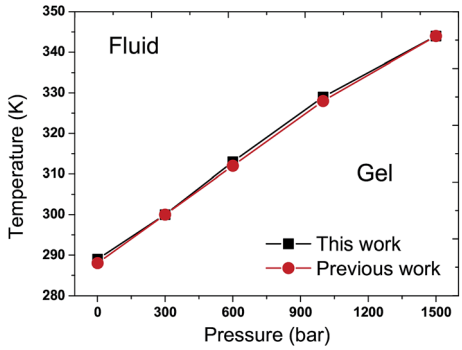

Fig. 3 T–p phase diagram of the pure DPPC bilayer. The black filled squares and red filled circles represent the results of this work and a previous work,[31] respectively. The T_m increases with the elevation of external pressure in the pure DPPC bilayer. The consistency between these two curves is noted.

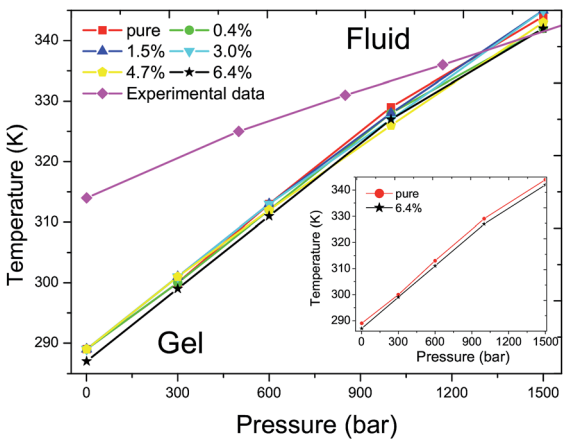

Fig. 4 T–p phase diagram of DPPC bilayers with different ratios of C_{60} under various external pressures. The red filled squares, green filled circles, blue filled equilateral triangles, cyan filled inverted triangles, yellow regular pentagons and black pentagrams represent the T_ms of DPPC bilayers with a ratio of C_{60} of 0%, 0.4%, 1.5%, 3%, 4.7% and 6.4%, respectively. The magenta filled rhombuses refer to experimental data of a pure DPPC bilayer.[42] The T_m increases with the elevation of external pressure with the presence of C_{60} in all of the simulations, similar to the pure DPPC bilayer case. The addition of a new component C_{60}, below a ratio of 4.7%, produces no significant impact on the T_m of the DPPC bilayer. However, the T_m decreases by approximately 2 K when the ratio of C_{60} increases to 6.4%, as shown in the inset figure.

increases to 6.4%. Also, the positive slope is controlled by the Clausius–Clapeyron equation and the deviation of the simulation result from the experimental data can be explained by the finite simulation time and the suppression of thermal undulations originating from periodic boundary conditions.[31]

More simulations were performed to study the relationship between T_m and external pressures. In a semi-isotropic pressure coupling way, different negative pressures were applied in the lateral direction while ambient pressure was enforced in the perpendicular direction. The specific pressure settings were (1) −5 bar in the lateral direction and 1 bar in the perpendicular direction; (2) −10 bar in the lateral direction and 1 bar in the perpendicular direction; and (3) −15 bar in the lateral direction and 1 bar in the perpendicular direction. Again, the *T*–*p* phase diagram was obtained in such a semi-isotropic pressure coupling way, as shown in Fig. 5. The result also suggests that the T_m increases with the increase of pressure in the lateral direction in all of the simulations. The vast majority of the differences of the T_ms for the various ratios of C_{60} and under different pressures are within 1 K compared with that of the pure DPPC bilayer. Accordingly, the T_m of the DPPC bilayer hardly changes in response to the presence of C_{60} in such a semi-isotropic coupling of pressure.

3.3 Radial distribution function *g*(*r*)

As shown in Fig. 6A, the radial distribution of the DPPC–DPPC molecules in the fluid phase at 325 K shows a long-range disordered distribution due to a disordered packing of the acyl chains in the fluid phase. In Fig. 6B, on the contrary, the radial distribution of the DPPC–DPPC molecules in the gel phase shows a long-range ordered distribution due to the ordered packing of the lipids in the gel phase. The various curves corresponding to the different ratios of C_{60} conform well to each other. Therefore, it can be concluded that the presence of C_{60} under a proportion of 6.4% does not disturb the radial distribution of the DPPC molecule in the lipid bilayer at ambient pressure. This probably can be explained by the limited amount of C_{60} present in the DPPC bilayer. The distortion of the lipid packing caused by the interaction between the C_{60} and DPPC molecules is too small to be observed in the radial distribution curves.

3.4 Lateral density profile

The lateral density profiles of a set of fluid DPPC bilayers at ambient pressure are shown in Fig. 7. The density curves of the DPPC bilayers and water intersect with each other at a distance of about 2.1 nm from the bilayer center. Moreover, the distance between the intersections of the DPPC bilayers and water can be used to estimate the thickness of the DPPC bilayer. In Fig. 7A and B, the distance between the intersections decreases with the increase of temperature, indicating that the thickness of the DPPC bilayer with relatively low ratios of C_{60} decreases with the temperature increase. The reduction in thickness can be explained by the bending and tilting of the acyl chains in the tail region with the temperature increase and therefore it can be concluded that the thickness of the DPPC bilayer is sensitive to temperature. However, in Fig. 7C–F, the distance between the intersections does not change with the increase of temperature, indicating that the thickness of the bilayer with a relatively high ratio of C_{60}–DPPC remains constant regardless of the temperature variation. Therefore, the different thicknesses with the elevation of temperature with different ratios of C_{60} suggest that

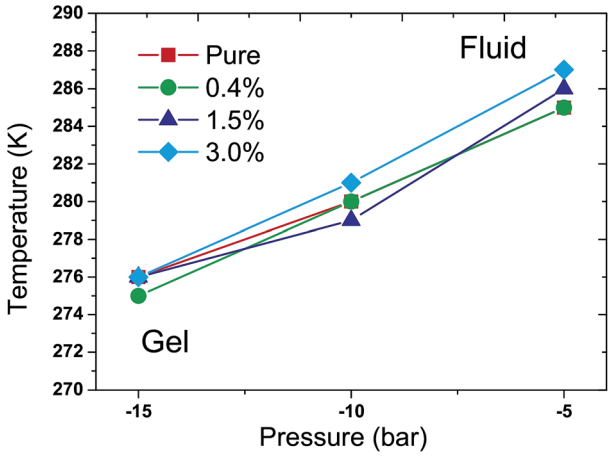

Fig. 5 *T*–*p* phase diagram of the DPPC bilayer with different ratios of C_{60} under various external pressures in a semi-isotropic coupling way. The red filled squares, green filled circles, blue filled triangles and cyan filled rhombuses represent the DPPC bilayer with C_{60}–DPPC ratios of 0%, 0.4%, 1.5% and 3.0%, respectively. In all of the simulations, the T_m increases with the elevation of pressure in the lateral direction. Moreover, the vast majority of the differences of the T_ms with various ratios of C_{60} and under different pressures are within 1 K compared with the pure DPPC bilayer case.

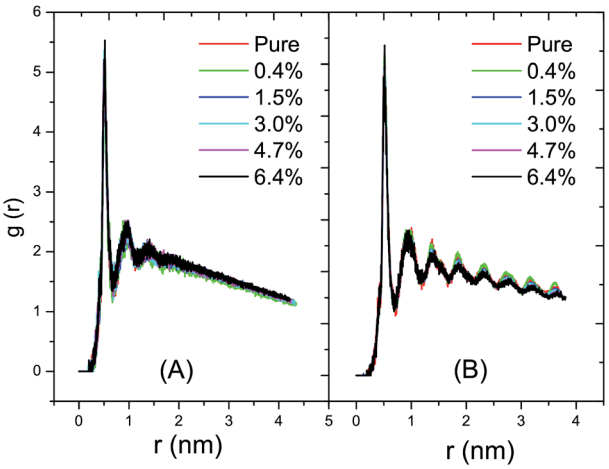

Fig. 6 The radial distribution functions, *g*(*r*), of the DPPC–DPPC molecules in the fluid and the gel phases at ambient pressure with various ratios of C_{60}. (A) The distribution function at 325 K with the DPPC bilayer in the fluid phase; and (B) the distribution function at 280 K with the DPPC bilayer in the gel phase. The red, green, blue, cyan, magenta and black lines represent the *g*(*r*) of the DPPC bilayers with ratios of C_{60} of 0%, 0.4%, 1.5%, 3.0%, 4.7% and 6.4%, respectively. A long-range disordered distribution and a long-range ordered distribution of the DPPC molecules emerges in the fluid phase and the gel phase, respectively. The radial distribution of the DPPC molecules in the bilayer does not change in the presence of a small amount of C_{60}.

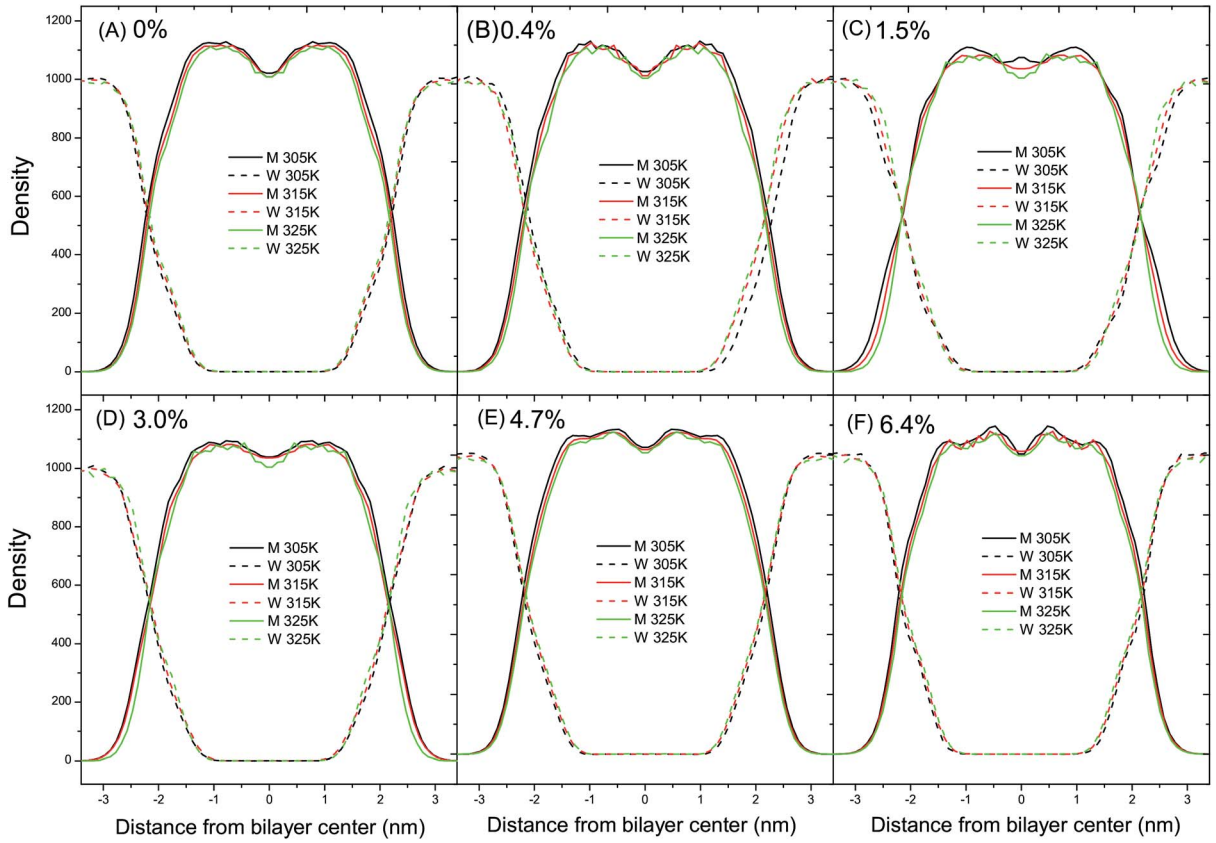

Fig. 7 Lateral density profiles of the fluid DPPC bilayer (M) and water (W) as a function of temperature at ambient pressure with different ratios of C_{60} of (A) 0%, (B) 0.4%, (C) 1.5%, (D) 3.0%, (E) 4.7% and (F) 6.4%. The black, red and green lines represent the density of M (solid lines) and W (dashed lines) at a temperature of 305 K, 315 K and 325 K, respectively. The thickness of the DPPC bilayer is sensitive to temperature, and the presence of C_{60} can stabilize the thickness of the DPPC bilayer. Moreover, the addition of C_{60} can produce a local influence on the radial distribution of the DPPC molecules.

the presence of C_{60} with a relatively high ratio can alleviate the sensitivity of the bilayer thickness to temperature. In other words, the presence of C_{60} with a relatively high ratio can stabilize the thickness of the DPPC bilayer. This can be understood based on the fact that the flexibility of the lipid tail is suppressed by the presence of C_{60} through steric hindrance. Accordingly, when the temperature increases, the tilting and bending of the lipid tail would become harder to take place, resulting in a constant bilayer thickness. Also, in Fig. 7A, the valley in the bilayer center remains almost unchanged with the increase of temperature. On the other hand, however, in Fig. 7B–F the density of the DPPC molecules in the bilayer center decreases with the increase of temperature. Such a difference suggests that the presence of C_{60} can impose a local influence on the lateral distribution of the DPPC molecules.

In the CG Martini force-field, the non-bonded interactions consist of LJ potential and Coulomb potential. The visual results with VMD showed that the interaction sites between C_{60} and the DPPC molecules locate in the CG beads C1 and Na, as shown in Fig. 1B. In the parameter setting of the CG Martini force-field, the parameters σ_{ij} between C1–C1, C1–CNP, Na–Na, and Na–CNP of the LJ potential energy function are all 0.47 nm. However, another parameter ε_{ij} between C1–CNP, C1–C1, Na–CNP, and Na–Na is 3.15 kJ mol^{-1}, 3.5 kJ mol^{-1}, 3.25 kJ mol^{-1} and 4.0 kJ mol^{-1}, respectively. The interaction strength between C1–CNP and Na–CNP is weaker than that of C1–C1 and Na–Na, respectively. This suggests that the presence of C_{60} weakens the non-bonding interactions, which can lead to a decrease in T_m. However, it has been reported that the presence of C_{60} also decreases the lateral diffusion coefficient of the DPPC molecules.[20] Our simulation also confirms a reduction of the lateral diffusion coefficient of the DPPC molecules with the addition of C_{60}. The reduced interactions between the molecules and the mobility of the DPPC molecules are possible explanations as to why the critical temperature, T_m, remains almost constant when C_{60} particles, below ratios of 4.7%, are introduced into the DPPC bilayer. A proper theoretical model is required to further the understanding of this phenomenon. At a ratio of C_{60} of 6.4%, the presence of C_{60} decreases the T_m of the DPPC bilayer by about 2 K, which is consistent with the result of the critical APL analysis in Fig. 2.

4 Conclusions

In this study, CGMD simulations have been performed to investigate the effect of C_{60} and its amount on the main

transition behavior and the distribution property of a DPPC bilayer at high pressure. The critical APL increases with the elevation of the amount of C_{60}. A critical area per lipid of 0.594 $\pm$ 0.002 nm^2 is obtained when the ratio of C_{60} reaches 6.4% while that of the pure bilayer case is 0.572 $\pm$ 0.002 nm^2. Our simulation results show that the T_m increases with the increase of external pressure. When the C_{60}–DPPC ratio is less than 4.7%, C_{60} particles exert no significant influence on the T_m of the DPPC bilayer. Also, the T_m decreases by about 2 K with a ratio of C_{60} of 6.4%. This suggests that the cytotoxicity of C_{60} is negligible from the point of view of the main transition when the ratio of C_{60} is less then 4.7%. Moreover, the *T*–*p* phase diagram of the DPPC bilayers with different ratios of C_{60} under various external pressures was obtained.

The radial distribution function and the lateral density profiles suggest that the presence of C_{60} produces no impact on the radial distribution of the DPPC molecules in the lipid bilayers but imposes a local influence on the lateral distribution of the DPPC molecules. The presence of C_{60} with a relatively high ratio decreases the sensitivity of the bilayer thickness to temperature and thus stabilizes the thickness of the DPPC bilayer.

Conflicts of interest

There are no conflicts to declare.

Acknowledgements

The authors acknowledge financial support from the National Natural Science Foundation of China (NSFC No. 61475196).

References

1 H. W. Kroto, J. R. Heath, S. C. O'Brien, R. F. Curl and R. E. Smalley, *Nature*, 1985, **318**, 162–163.
2 J. Coro, M. Suárez, L. S. Silva, K. I. Eguiluz and G. R. Salazar-Banda, *Int. J. Hydrogen Energy*, 2016, **41**, 17944–17959.
3 S. Z. Mousavi, S. Nafisi and H. I. Maibach, *Nanomedicine*, 2017, **13**, 1071–1087.
4 I. Rasović, *Mater. Sci. Technol.*, 2016, **33**, 777–794.
5 A. Kausar, *Polym.-Plast. Technol. Eng.*, 2017, **56**, 594–605.
6 K. Aschberger, H. J. Johnston, V. Stone, R. J. Aitken, C. L. Tran, S. M. Hankin, S. A. Peters and F. M. Christensen, *Regul. Toxicol. Pharmacol.*, 2010, **58**, 455–473.
7 S. H. Friedman, D. L. DeCamp, R. P. Sijbesma, G. Srdanov, F. Wudl and G. L. Kenyon, *J. Am. Chem. Soc.*, 1993, **115**, 6506–6509.
8 R. Sijbesma, G. Sdanovr, F. Wudl, J. A. Castoro, C. Wilkins, S. H. Friedman, D. L. Decamp and G. L. Kenyon, *ChemInform*, 1993, **115**, 6510–6512.
9 S. Bosi, T. D. Ros, G. Spalluto and M. Prato, *Eur. J. Med. Chem.*, 2003, **38**, 913–923.
10 G. L. Marcorin, T. D. Ros, S. Castellano, G. Stefancich, I. Bonin, S. Miertus and M. Prato, *Org. Lett.*, 2000, **2**, 3955–3958.
11 P. Krusic, E. Wasserman, P. Keizer, J. Morton and K. Preston, *Science*, 1991, **254**, 1183–1185.
12 R. Bakry, R. M. Vallant, M. Najam-ul Haq, M. Rainer, Z. Szabo, C. W. Huck and G. K. Bonn, *Int. J. Nanomed.*, 2007, **2**, 639–649.
13 Z. Markovic and V. Trajkovic, *Biomaterials*, 2008, **29**, 3561–3573.
14 T. Y. Zakharian, A. Seryshev, B. Sitharaman, B. E. Gilbert, V. Knight and L. J. Wilson, *J. Am. Chem. Soc.*, 2005, **127**, 12508–12509.
15 F. Lu, S. A. Haque, S.-T. Yang, P. G. Luo, L. Gu, A. Kitaygorodskiy, H. Li, S. Lacher and Y.-P. Sun, *J. Phys. Chem. C*, 2009, **113**, 17768–17773.
16 P. Chaudhuri, A. Paraskar, S. Soni, R. A. Mashelkar and S. Sengupta, *ACS Nano*, 2009, **3**, 2505–2514.
17 Y. Tabata, Y. Murakami and Y. Ikada, *Jpn. J. Cancer Res.*, 1997, **88**, 1108–1116.
18 S. K. Sharma, Y. C. Long and M. R. Hamblin, *Nanomedicine*, 2011, **6**, 1813–1825.
19 L. Li, H. Davande, D. Bedrov and G. D. Smith, *J. Phys. Chem. B*, 2007, **111**, 4067–4072.
20 J. Wong-Ekkabut, S. Baoukina, W. Triampo, I.-M. Tang, D. P. Tieleman and L. Monticelli, *Nat. Nanotechnol.*, 2008, **3**, 363–368.
21 C. Chiu, W. Shinoda, R. H. Devane and S. O. Nielsen, *Soft Matter*, 2012, **8**, 9610–9616.
22 W. D. Tian, K. Chen and Y. Q. Ma, *RSC Adv.*, 2014, **4**, 30215–30220.
23 N. Nisoh, M. Karttunen, L. Monticelli and J. Wongekkabut, *RSC Adv.*, 2015, **5**, 11676–11685.
24 J. Zhou, D. Liang and S. Contera, *Nanoscale*, 2015, **7**, 17102–17108.
25 Y. K. Cherniavskyi, C. Ramseyer and S. O. Yesylevskyy, *Phys. Chem. Chem. Phys.*, 2016, **18**, 278–284.
26 K. Jacobson and D. Papahadjopoulos, *Biochemistry*, 1975, **14**, 152–161.
27 J. Barnoud, G. Rossi and L. Monticelli, *Phys. Rev. Lett.*, 2014, **112**, 290a.
28 A. Ikeda, K. Kiguchi, T. Shigematsu, K. Nobusawa, J.-i. Kikuchi and M. Akiyama, *Chem. Commun.*, 2011, **47**, 12095–12097.
29 G. Rossi, J. Barnoud and L. Monticelli, *Phys. Scr.*, 2013, **87**, 058053–058062.
30 S. J. Marrink, A. H. de Vries and D. P. Tieleman, *Biochim. Biophys. Acta, Biomembr.*, 2009, **1788**, 149–168.
31 K. Lai, B. Wang, Y. Zhang and Y. Zhang, *Phys. Chem. Chem. Phys.*, 2012, **14**, 5744–5752.
32 R. Kociurzynski, M. Pannuzzo and R. A. Böckmann, *Langmuir*, 2015, **31**, 9379–9387.
33 J. Prates Ramalho, P. Gkeka and L. Sarkisov, *Langmuir*, 2011, **27**, 3723–3730.
34 R. M. Venable, B. R. Brooks and R. W. Pastor, *J. Chem. Phys.*, 2000, **112**, 4822–4832.
35 S. J. Marrink, H. J. Risselada, S. Yefimov, D. P. Tieleman and A. H. de Vries, *J. Phys. Chem. B*, 2007, **111**, 7812–7824.
36 S. J. Marrink, A. H. D. Vries and A. E. Mark, *J. Phys. Chem. B*, 2004, **108**, 750–760.

37 T. A. Wassenaar, H. I. Ingólfsson, R. A. Böckmann, D. P. Tieleman and S. J. Marrink, *J. Chem. Theory Comput.*, 2015, **11**, 2144–2155.
38 H. J. C. Berendsen, D. van der Spoel and R. van Drunen, *Comput. Phys. Commun.*, 1995, **91**, 43–56.
39 E. Lindahl, B. Hess and D. van der Spoel, *J. Mol. Model.*, 2001, **7**, 306–317.
40 H. J. C. Berendsen, J. P. M. Postma, W. F. V. Gunsteren, A. Dinola and J. R. Haak, *J. Chem. Phys.*, 1984, **81**, 3684–3690.
41 W. Humphrey, A. Dalke and K. Schulten, *J. Mol. Graphics*, 1996, **14**, 33–38.
42 S. Potekhin, A. Senin, N. Abdurakhmanov and R. Khusainova, *Biochim. Biophys. Acta, Biomembr.*, 2008, **1778**, 2588–2593.
43 S. J. Marrink, J. Risselada and A. E. Mark, *Chem. Phys. Lipids*, 2005, **135**, 223–244.